



Torsional Fatigue Failure of Additively Manufactured Stainless Steel of Reduced Specimen Size

SANNA F. SIDDIQUI,^{1,4} FIRAT IRMAK,² ABIODUN A. FASORO,³ and ALI P. GORDON²

1.—Mechanical Engineering Department, Florida Polytechnic University, Lakeland, FL 33805, USA. 2.—Department of Mechanical and Aerospace Engineering, University of Central Florida, Orlando, FL 32816, USA. 3.—Department of Mechanical and Manufacturing Engineering, Tennessee State University, Nashville, TN 37209, USA. 4.—e-mail: ssiddiqui@floridapoly.edu

The torsional fatigue response of as-built direct metal laser sintered (DMLS) stainless steel (SS) GP1 of reduced specimen size and horizontal build orientation subjected to cyclic loading at a highly plastic shear strain has been investigated. The average shear modulus, G , was found to be 55.36 GPa, with shear stress history revealing cyclic hardening to stabilization and softening to fracture. Findings suggest that stainless steel GP1 of reduced specimen size experiences fatigue crack initiation at voids near the surface, resulting in a star-spline brittle fracture response, and premature torsional fatigue failure within the low cycle fatigue regime. A noninteraction deformation constitutive model through finite element simulations has been used to successfully simulate the deformation response of the gage section under torsional fatigue conditions.

INTRODUCTION

Materials used in aerospace components, which are subject to a multiaxial stress state, must be durable under both axial and torsional fatigue loading conditions. Torsional fatigue failure, which is driven by a materials' inability to withstand cyclic shear stresses, has caused failure of aerospace engine components, machine shafts, railways, and much more. With the additive manufacturing of these components on the rise, it is vital to ensure that the additive manufacturing process produces components that meet/exceed the shear performance of current parts made through subtractive machining techniques. Studies have investigated the torsional fatigue response of SS 17-4PH, developed through conventional subtractive machining techniques, including failure due to cyclic shearing in the very high cycle fatigue regime,¹ as well as the role of small defects in the fatigue limits of SS 17-4PH through rotating-bending and axial torsional

testing,^{2,3} carried out into the high cycle fatigue regime. Considerable research has been reported on the axial monotonic and cyclic response of additively manufactured metals, however the cyclic shear failure response of these as-manufactured parts is not understood. Studies have reported the monotonic torsion and torsional fatigue response of AM Ti-6Al-4V,⁴ monotonic shear response of three-dimensionally (3D)-printed polylactic acid (PLA),⁵ and Poisson's ratio variation with build orientation has been reported for an AM stainless steel alloy.⁶ More recently, a preliminary study on the monotonic torsion and torsional fatigue response of direct metal laser sintered (DMLS) GP1 SS has been reported for conventionally sized ASTM test specimens.⁷ The key distinction between the current study and the earlier reported study⁷ is the specimen size. The current study investigates how additively manufactured specimens of reduced specimen size exhibit varying torsional fatigue failure response (i.e., life, fracture response, etc.), while ensuring cost savings through the AM process. Most studies in the area of AM stainless steel 17-4PH or stainless steel GP1 have focused upon assessing its axial tensile and compressive response^{8–12} along with the axial low cycle and high cycle fatigue

Previous Affiliations: Sanna F. Siddiqui—Department of Mechanical and Aerospace Engineering, University of Central Florida, Orlando, FL 32816, USA. Abiodun A. Fasoro—Manufacturing Engineering Department, Central State University, Wilberforce, OH 45384, USA.

response.^{13–18} This study provides insight into the torsional fatigue response (i.e., life, hardening/softening, fracture mechanism, shear modulus, etc.) of additively manufactured stainless steel GP1 of reduced specimen size. It further assesses the applicability of a viscoplasticity model^{19,20} in effectively simulating the cyclic hysteresis response exhibited by this material.

Accurate simulations are essential in the research and development of critical components that experience extreme mechanical loads at room and elevated temperatures. A robust and efficient constitutive model is needed to perform accurate and meaningful simulations at the component scale. This constitutive model needs to consider temperature, rate, and history dependence happening at the material level. Earlier studies^{21,22} have presented the success of a noninteraction (NI) model unifying distinct elastic, plastic, and creep components in conjunction with general-purpose finite element programs.

A noninteraction (NI) method is used as the deformation modeling approach for constitutive modeling of the cyclic shear stress deformation in this study. The NI model simplifies the total strain into its respective elastic and plastic components, such that

$$\varepsilon_{\text{total}} = \varepsilon_{\text{el}}(\sigma, T) + \varepsilon_{\text{pl}}(\sigma, T), \quad (1)$$

where $\varepsilon_{\text{total}}$ is the total strain, ε_{el} is the elastic strain component, ε_{pl} is the time-independent plastic strain component, σ is the stress tensor, T is temperature, and t is time, as depicted in Eq. 1. The deformation model is constructed by using a methodical process. The cyclic Ramberg–Osgood model²³ is determined by the mid-life cyclic stress–strain curves from low cycle fatigue (LCF) experiments.

$$\varepsilon_a = \frac{\sigma_a}{E} + \left(\frac{\sigma_a}{K'}\right)^{\frac{1}{n'}} \quad (2)$$

Here, ε_a is the strain amplitude, σ_a is the stress amplitude, E is the elastic modulus, and K' and n' are the cyclic strain hardening coefficient and exponent, which exhibit temperature dependence. For the purpose of this study, as all experiments were conducted at room temperature, temperature

was not considered within the model. Hysteresis curve generation was achieved using the Masing nonlinear hardening model,²⁴ i.e.,

$$\Delta\varepsilon = \frac{\Delta\sigma}{E} + 2\left(\frac{\Delta\sigma}{2K'}\right)^{\frac{1}{n'}} \quad (3)$$

for stabilized cyclic conditions, where $\Delta\varepsilon$ is the strain range and $\Delta\sigma$ is the stress range, as depicted in Eq. 3. The nonlinear kinematic hardening (NLKH) model was developed by estimating the back stress of the plastic response as a set of multiple superimposed Armstrong–Fredrick (A–F) kinematic hardening models and a component for change in temperature.²⁵

$$\dot{X} = \frac{2}{3} \sum_{i=1}^3 C_i \dot{\varepsilon}^{\text{pl}} - \gamma_i X_i \dot{p} + \frac{1}{C_i} \frac{dC_i}{d\theta} \dot{\theta} X_i. \quad (4)$$

The NLKH model defines \dot{X} as the rate of change of the back stress tensor, C_i , γ_i , and X_i as the hardening modulus, hardening modulus rate, and back stress tensor of the three superimposed A–F models, respectively. Here, k is defined as the initial yield stress, $\dot{\varepsilon}^{\text{pl}}$ is the plastic strain rate tensor, \dot{p} is the change of the accumulated equivalent plastic strain with respect to time, θ is the temperature, and $\dot{\theta}$ is the temperature rate. In practice, the C_i terms affect the slope of the stress–strain hysteresis loop, and the γ_i terms change the decay of the slopes, allowing for plastic memory hardening over subsequent cycles. Table I summarizes the model parameters, and the effect each material constant produces.

The constant determination process is decomposed into three different steps. The first step employs a slope method to find C_1 , C_2 , and C_3 :

$$C_i = \frac{K' \left(\Delta\varepsilon_{\text{offset},i+1}^{n'} - \Delta\varepsilon_{\text{offset},i}^{n'} \right)}{2^{n'-1} (\Delta\varepsilon_{\text{offset},i+1} - \Delta\varepsilon_{\text{offset},i})}, \quad (5)$$

where the bounding points are defined as

$$\Delta\varepsilon_{\text{offset},i} = [0.00001 \quad 0.0002 \quad 0.002 \quad 0.0038] \quad (6)$$

The second step includes analytically approximating the k constant as the yield stress of the hysteresis loop where the plastic strain amplitude is very low, on the order of

Table I. Description of material constants used in model

| Constant | Unit | Model | Plot abscissa-axis plot ordinate-axis | Primary effect |
|------------|------|------------|--|----------------------------|
| K' | MPa | Cyclic R–O | Plastic strain (mm/mm) versus stress (MPa) | Height/magnitude curvature |
| n' | – | | | |
| C_i | MPa | NLKH | Plastic strain (mm/mm) versus stress (MPa) | Slope of the segments |
| γ_i | – | | | Decay of the segments |
| K | MPa | | | Proportional limit |

$$k = K'(0.00001)^{n'} \quad (7)$$

For approximating the linearized back stress for a set of stress ranges and plastic strain range points, γ_1 , γ_2 , and γ_3 ; statistical regression or analytical methods are employed in the last step, i.e., Equation 8,

$$\frac{\Delta\sigma}{2} - k = \frac{C_1}{\gamma_1} \tanh\left(\gamma_1 \frac{\Delta\varepsilon^{pl}}{2}\right) + \frac{C_2}{\gamma_2} \tanh\left(\gamma_2 \frac{\Delta\varepsilon^{pl}}{2}\right) + \frac{C_3}{\gamma_3} \tanh\left(\gamma_3 \frac{\Delta\varepsilon^{pl}}{2}\right). \quad (8)$$

The stress ranges are obtained using plastic strain range values of 0.05% thru 0.1% in increments of 0.01%, and 0.2% thru 0.5% in increments of 0.1%. Least-squares regression is employed to fit the γ constants. Further detail regarding the constitutive model used in this study can be found in Ref. 21.

This study is novel in that it uses this noninteraction (NI) model in conjunction with a finite element ANSYS model to successfully simulate the torsional fatigue deformation response of stainless steel GP1 of reduced specimen size.

EXPERIMENTAL

The experimental approach and specimen design were tailored to enable assessment of the mechanical response of DMLS SS GP1 under cyclic shear loading conditions at high plastic shear strain, in addition to using a reduced specimen size to promote cost savings in the additive manufacturing of this material. The specimen design is as shown in Fig. 1a, with total length of 81.28 mm, gauge length of 25.4 mm, and inner gauge diameter of 5.08 mm. A three-pronged gripping design was machined in the shaft section prior to torsional fatigue testing, which is shown in Fig. 1b, in which machining marks in the radial section of the specimen were removed using a 330 M grit sandpaper. The specimens were manufactured along three build orientations in the horizontal build plane, -5° from the x -axis, 45° in the xy plane, and -5° from the y -axis, referred to as (X), (XY45), and (Y) throughout the text. To ensure repeatability in torsional fatigue findings, a total of five specimens manufactured along the horizontal build orientation [two (X), one (XY45), and two (Y)] were subjected to torsional fatigue tests. The EOS M280 direct metal laser sintering (DMLS) system was used to manufacture the specimens, using a layer thickness of $20 \mu\text{m}$ in a nitrogen gas chamber environment, in which the gauge section was left in the as-built condition prior to testing. EOS-recommended optimized processing parameters for stainless steel GP1 were used to manufacture the specimens.

The specimens were subject to completely reversible ($R_\phi = -1$) torsional fatigue tests at an angular rate of $1.654^\circ/\text{s}$, data acquisition rate of 10 Hz, and

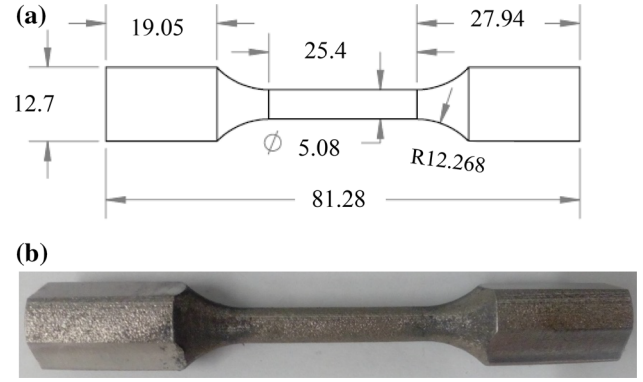


Fig. 1. Reduced torsion specimen (a) geometry (mm),¹⁷ and (b) after machining three prongs in the gripping section prior to torsional fatigue testing.

angle of twist range of 30° , cycling between $+15^\circ$ and -15° , using the MTS EM Bionix Torsion Test Device. Experimental results were recorded as torque, T , versus angle of twist, ϕ , which were converted to shear stress, τ , and shear strain, γ , using the following relationships:

$$\tau = \frac{Tr}{J}, \quad (9)$$

$$\gamma = \frac{\phi r}{L}, \quad (10)$$

$$J = \frac{\pi r^4}{2}. \quad (11)$$

The polar moment of inertia, J , was determined from the radius, r , of the inner gauge section of the specimen, and the length, L , of the gauge section. Experimental findings (i.e., shear stress cyclic deformation with time) are further simulated using a noninteraction deformation constitutive model, discussed in the “Introduction” section.

RESULTS

The experimental results from torsional fatigue testing of additively manufactured reduced test specimens are presented and correlated with the exhibited fracture response. A superposition of the first and stabilized hysteresis response for each build orientation, manufactured in the horizontal plane, is presented in Fig. 2a and b, from which the following observations were made: First, the amount of plasticity captured during the initial and mid-life cycles are significant, as compared with conventional torsion specimens, presented in an earlier study,⁷ which were subjected to the same experimental conditions. This suggests that a reduction in the test specimen size, specifically the inner gauge diameter, allows for a more pronounced impact of plasticity effects, which may dominate failure in additively manufactured specimens. Second, under the assumption that these materials

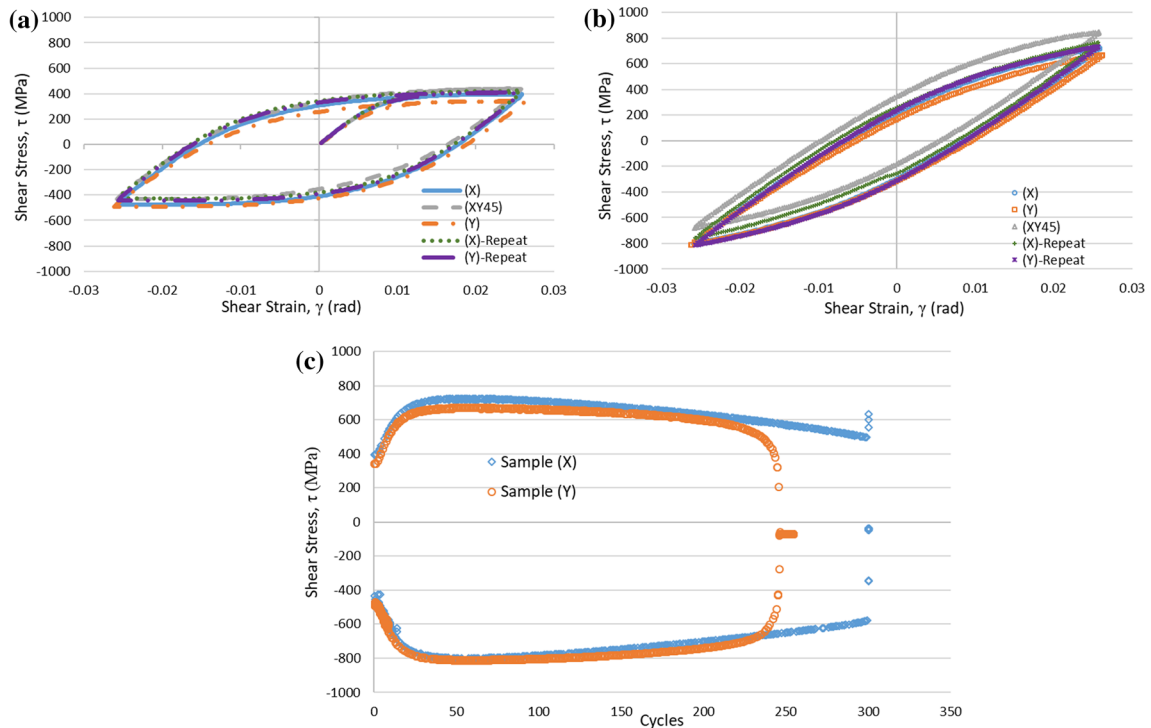


Fig. 2. Torsion fatigue testing of reduced test specimens: (a) first cycle shear stress versus shear strain hysteresis response, (b) stabilized cycle shear stress versus shear strain hysteresis response, and (c) shear stress history for (X) and (Y) orientations.¹⁷

exhibit isotropic material behavior for build orientations in the xy plane, the overlay of cycles across build orientation, depicted in Fig. 2, should each capture a similar cyclic response. However, slight variations exist, which may be attributed to an induced slight tensile/compressive mean stress on the specimen during specimen gripping, under completely reversible ($R_\phi = -1$) torsional fatigue conditions. These small variations may also be attributed to variation between batches, as a second set of samples of X and Y orientation were subjected to torsional fatigue tests to validate experimental findings. These qualitative observations exhibited by the first and stabilized cycles are explored further through characterization of the torsional properties exhibited by each cycle.

A comparison of the shear stress range from the first cycle to the stabilized cycle in Fig. 2c reveals material hardening during completely reversed torsional fatigue testing. An analysis of the shear stress histories for these specimens reveals hardening to stabilization, followed by softening of the material just before fracture. This characteristic hardening/softening behavior was also observed for DMLS GP1 SS subject to axial low cycle fatigue tests.^{13,17} This finding is comparable to the hardening response to stabilization observed in an earlier reported study on conventional torsion specimens as well.⁷

The torsional properties including the shear modulus, G , shear stress range, $\Delta\tau$, total shear strain range, $\Delta\gamma$, mean shear stress, τ_m , elastic

shear strain range, $\Delta\gamma_e$, and plastic shear strain range, $\Delta\gamma_p$ are presented in Table II. The shear modulus is found to reduce from the initial to mid-life cycles for all build orientations. A comparison has been done between the shear modulus obtained from first cycle measurements for DMLS GP1 SS and other stainless steel alloys (i.e., cast SS 17-4PH and SS 304). However, it is important to note that, while the chemical composition of SS GP1 and SS 17-4PH are similar, their mechanical response has been shown to vary, as a result of varying phase composition makeup.²⁶ The shear modulus reported for solution-annealed and heat-treated SS 17-4PH has been reported to be 79.07 GPa²⁷ and 86 GPa for SS 304,²⁸ and ~ 50 GPa for DMLS GP1 SS of conventional test specimen size (i.e., gauge diameter of 6.096 mm).⁷ From Table II, it is evident that the shear modulus of DMLS GP1 SS, for build orientations in the xy plane, is considerably lower than that reported for other stainless steel alloys. This suggests that, under the tested shear fatigue loading conditions, the material performance of DMLS GP1 SS is limited, which may be attributed to the limited shear stress carrying capacity of the as-built rough surface of DMLS GP1 SS, as has been reported by other studies on AM materials.⁴ Also evident is the large plastic shear strain range within the first cycle, approximately 0.033, which reduces with cycling to stabilization, to approximately 0.015. Overall, small variations are observed in torsional properties obtained across build orientation, likely attributed to variations between

Table II. Cyclic torsional properties (rounded) for DMLS SS GP1, subject to completely reversible ($R_\phi = -1$) torsional fatigue tests

| Orientation | Shear stress range, $\Delta\tau$ (MPa) | Mean shear stress, τ_m (MPa) | Plastic shear strain range, $\Delta\gamma_p$ (rad) | Elastic shear strain range, $\Delta\gamma_e$ (rad) | Total shear strain range, $\Delta\gamma$ (rad) | Shear modulus, G (GPa) |
|---|--|-----------------------------------|--|--|--|--------------------------|
| <i>First cycle-reduced test specimen</i> | | | | | | |
| X | 872.5 | - 41.47 | 0.0332 | 0.0160 | 0.0492 | 54.56 |
| Y | 830.8 | - 76.3 | 0.0331 | 0.0146 | 0.0477 | 56.94 |
| XY45° | 870.97 | 2.31 | 0.0328 | 0.0141 | 0.0469 | 61.68 |
| X-Repeat | 838.5 | - 7.5 | 0.0337 | 0.0161 | 0.0498 | 52 |
| Y-Repeat | 847.5 | - 20.09 | 0.0334 | 0.0164 | 0.0498 | 51.64 |
| Average | - | - | - | - | - | 55.364 ± 4.129 |
| <i>Stabilized cycle-reduced test specimen</i> | | | | | | |
| X | 1525.29 | - 37.7 | 0.0150 | 0.0367 | 0.0517 | 41.56 |
| Y | 1481.67 | - 71.18 | 0.0147 | 0.0377 | 0.0524 | 39.31 |
| XY45° | 1527.62 | 85.22 | 0.0152 | 0.0363 | 0.0515 | 42.03 |
| X-Repeat | 1522.93 | 2.53 | 0.0154 | 0.0359 | 0.0513 | 42.45 |
| Y-Repeat | 1550.24 | - 39.2 | 0.0154 | 0.0359 | 0.0513 | 43.17 |
| Average | - | - | - | - | - | 41.704 ± 1.463 |
| Reference | Material | | Shear modulus, G (GPa) | | | |
| Current study | DMLS SS GP1 | | 55.364 ± 4.129 | | | |
| Ref. 27 | Solution-annealed and heat-treated SS 17-4PH | | 79.07 | | | |
| Ref. 28 | Cast SS 304L | | 86 | | | |

batches, as a second set of samples of X and Y orientation were subjected to torsional fatigue tests to validate experimental findings. The results presented in Table II support the assumption that this material exhibits isotropic material behavior within the xy horizontal build plane.

It is critical to determine the durability of such components when subject to realistic service conditions (i.e., torsional fatigue). Therefore, the shear stress history for reduced torsion specimens manufactured along the (X) and (Y) orientations is as presented in Fig. 2c. There is a considerable reduction in the number of cycles to failure for these specimens, which may be attributed to their reduced geometry (i.e., inner gauge diameter/length), as opposed to torsional specimens of conventional size (i.e., inner gauge length of 50.038 mm, inner gauge diameter of 6.096 mm), reported in earlier findings.⁷

An analysis of the fracture response for these specimens, subject to completely reversed torsional fatigue, reveals a brittle fracture response. Figure 3 captures the fracture response of these specimens, from which a star-spline brittle fracture response is observed, suggesting unstable crack propagation due to the presence of internal voids/porosity, an outcome of the AM process, resulting in sudden and catastrophic failure of the specimens. To further assess the mechanisms driving torsional fatigue failure of these specimens, scanning electron microscopy (SEM) images were taken of crack initiation and propagation within each specimen shown

within Fig. 4. SEM images were taken using an Hitachi SU3500 microscope in secondary electron (SE) mode at beam energy of 20.0 kV, spot intensity of 30, and working distance of 6.4 mm to 6.7 mm. It can be seen that multiple cracks have been initiated at voids near the as-built surface of the specimen, suggesting that surface roughness initiated the brittle fracture response exhibited by these specimens.

CONSTITUTIVE MODELING

A finite element model was developed to calculate the deformation of the material for a cylindrical gauge section using the noninteraction model, presented in “Introduction” section. ANSYS Mechanical APDL 19.2 was employed to execute this finite element code on a multielement model.¹⁹ For applying the angle of torsion, a remote displacement control method is utilized on the cylindrical geometry which has a gauge length of 25.4 mm. To allow expansion or contraction, one face of the cylinder was unconstrained while the other face was fixed supported, replicating the experimental setup used during torsional fatigue testing, in which one side of the specimen was fixed while the other was rotated, as shown in Fig. 5b. Second-order (quadratic) elements are used to mesh the cylindrical geometry. A total of 15,640 elements are created to carry out the simulations.

The constitutive modeling approach presented in the “Introduction” section was used to model the shear stress response of DMLS GP1 SS over time.

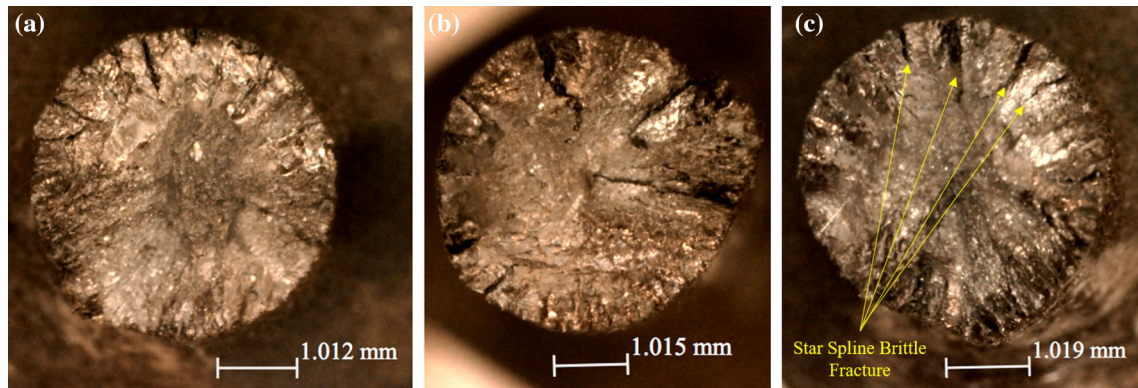


Fig. 3. Optical micrograph images of fracture surfaces after completely reversed ($R_\phi = -1$) torsional fatigue tests on reduced torsion fatigue specimens, in which clear brittle fracture response is evident at varying magnifications ($25\times$ to $30\times$): (a) X-orientation, (b) Y-orientation, and (c) XY45° orientation.¹⁷

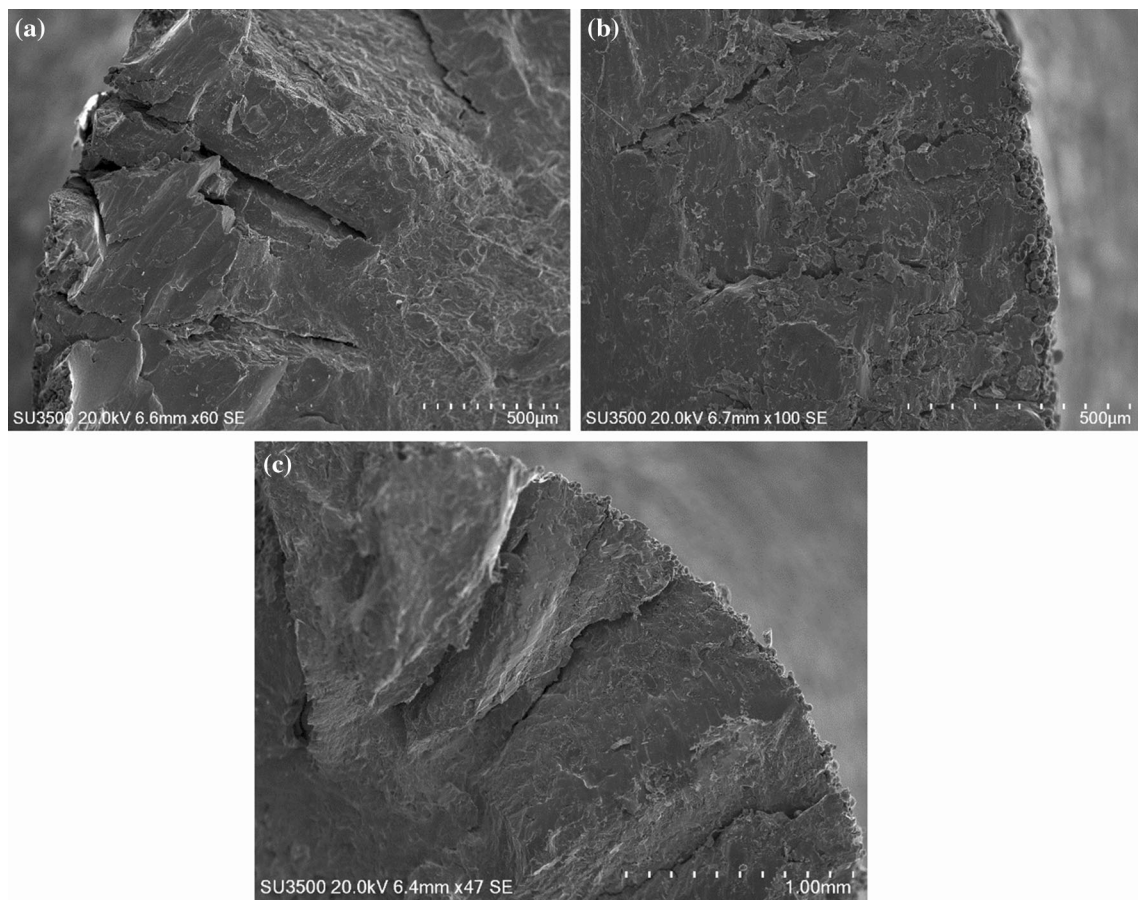


Fig. 4. SEM images capturing brittle fracture surface with cracks initiated at voids near the surface: (a) sample 2, (b) sample 10, and (c) sample 17.

The constant determination process utilized to establish values for the cyclic Ramberg–Osgood and nonlinear kinematic hardening models is as shown in Table III. All the values presented here are for room-temperature conditions. The model is compared with experimental data for the x -oriented specimen in Fig. 5a, in which the model simulates the peak shear stress very accurately, while it

slightly underpredicts the valley stress. The deformed shape of the specimen gauge section obtained by FE analysis is shown in Fig. 5b. The deformation varies from 0 m at the fixed end of the specimen to 0.0002553 m at the far end of the specimen where the torque is applied. Overall, this model has been used to successfully simulate the

Table III. Optimized constants determined from FEM simulation of torsional fatigue response of DMLS SS GP1

| Constants | Model | Unit | Value |
|------------|------------|------|-----------|
| K' | Cyclic R-O | MPa | 1096 |
| n' | | – | – 0.1027 |
| C_1 | NLKH | MPa | 1,186,814 |
| γ_1 | | – | – 14,584 |
| C_2 | | MPa | 126,192 |
| γ_2 | | – | – 1312 |
| C_3 | | MPa | 40,830 |
| γ_3 | | – | – 236 |
| K | | MPa | 336 |

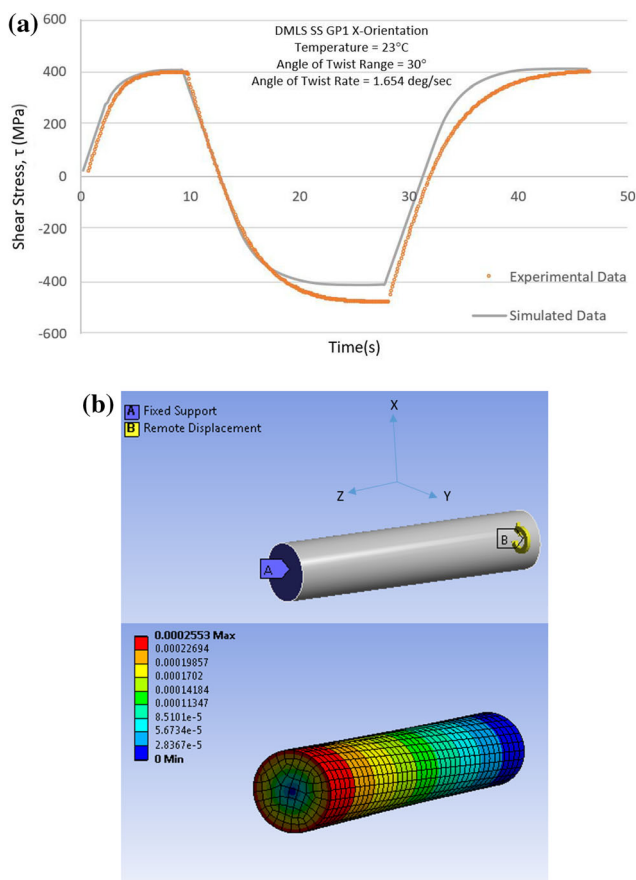


Fig. 5. DMLS SS GP1: (a) Modeling of shear stress, τ , variation with time compared with experimental data and (b) specimen deformation (in meters) during finite element modeling simulation.

experimental shear stress response exhibited by an as-built additively manufactured stainless steel subject to torsional fatigue loading conditions.

CONCLUSION

Additive manufacturing techniques must be designed such that the resulting aerospace parts can withstand multiaxial (i.e., axial and torsional)

loading conditions, in order to replace current, conventional subtractive manufacturing techniques. This study is novel in that it assessed the torsional fatigue response of as-built additively manufactured stainless steel GP1, of reduced specimen size, when subjected to cyclic loading at a highly plastic shear strain, and supported experimental findings through application of a noninteraction deformation constitutive model. Experimental findings suggest that as-built DMLS SS GP1 of horizontal build orientation experiences premature failure, hardening to stabilization, and softening to fracture, thereby resulting in a brittle fracture for all specimens tested. Average shear modulus was found to be $G = 55.36$ GPa for the horizontal build orientation. The noninteraction deformation constitutive model has been used to successfully simulate the shear stress response of additively manufactured metal materials.

ACKNOWLEDGEMENTS

This material is based upon work supported by the National Science Foundation Graduate Research Fellowship Program under Grant No. (1144246) awarded to Sanna F. Siddiqui. Abiodun A. Fasoro would like to acknowledge the financial support of the Air Force Research Collaboration Program (RCP) through AFRL/UTC/Clarkson Aerospace. DMLS manufacturing of specimens used in this study was carried out using the EOS M280 system in the Manufacturing Engineering Department at Central State University. The authors would also like to acknowledge Mr. Samuel Kleespies.

REFERENCES

1. B.M. Schonbauer, K. Yanase, and M. Endo, in *Proceedings of Seventh International Conference on Very High Cycle Fatigue*, (2017).
2. B.M. Schonbauer, H. Mayer, K. Yanase, and M. Endo, *Procedia Struct. Integrity* 7, 492 (2017).
3. Y. Ochi, T. Matsumura, K. Masaki, and S. Yoshida, *Fatigue Fracture Eng (Struct: Mater)*, 2002).
4. A. Fatemi, R. Molaei, S. Sharifimehr, N. Shamsaei, and N. Phan, *Int. J. Fatigue* 99, 187 (2017).
5. J. Torres, J. Cotel, J. Karl, and A.P. Gordon, *JOM* 67, 1183 (2015).
6. L. Hitzler, J. Hirsch, B. Heine, M. Merkel, W. Hall, and A. Oschner, *Materials* 10, 1 (2017).
7. S.F. Siddiqui, A.A. Fasoro, and A.P. Gordon, in *Proceedings of the ASME 2018 Turbo Expo Turbomachinery Technical Conference & Exposition, GT2018-76831*, June 11–15, 2018, Oslo, Norway (2018).
8. A. Yadollahi, N. Shamsaei, S.M. Thompson, A. Elwany, L. Bian, and M. Mahmoudi, in *Proceedings of the 26th International Solid Freeform Fabrication Symposium*, Austin, TX, 721 (2015).
9. M. Mahmoudi, A. Elwany, A. Yadollahi, S.M. Thompson, L. Bian, and N. Shamsaei, *Rapid Prototyp. J.* (2017). <https://doi.org/10.1108/rpj-12-2015-0192>.
10. W.E. Luecke and J.A. Slotwinski, *J. Res. Natl. Inst. Standards Technol.* 119, 398 (2014).

11. L. Facchini, N. Vicente, I. Lonardelli, E. Magalini, P. Robbotti, and A. Molinari, *Adv. Eng. Mater.* 12, 184 (2010).
12. S.F. Siddiqui, N. O’Nora, A.A. Fasoro, and A.P. Gordon, in *Proceedings of the ASME 2017 International Mechanical Engineering Congress & Exposition*, IMECE2017-71561, Nov 3–9, 2017, Tampa, FL (2017).
13. A. Yadollahi, N. Shamsaei, S.M. Thompson, A. Elwany, and L. Bian, *Int. J. Fatigue* 94, 218 (2017).
14. H.A. Stoffregen, K. Butterweck, and E. Abele, in *25th Solid Freeform Fabrication Symposium*, 635 (2014).
15. J.T. Sehart and G. Witt, in *Proceedings of the 36th International MATADOR Conference*, 385 (2010).
16. W. Everhart, E. Sawyer, T. Neidt, J. Dinardo, and B. Brown, *J. Mater. Sci.* 51, 3836 (2016).
17. S.F. Siddiqui, *Characterization of Anisotropic Mechanical Performance of As-Built Additively Manufactured Metals*, PhD Dissertation. University of Central Florida (2018).
18. L. Carneiro, B. Jalalahmadi, A. Ashtekar, and Y. Jiang, *Int. J. Fatigue* 123, 22 (2019).
19. F. Irmak, *A Flexible Physics-Base Lifting Method for Metals under Creep and Thermomechanical Fatigue*. Master’s Thesis. University of Central Florida, (2017).
20. N.R. O’Nora, *Compendium of Thermoviscoplasticity Modeling Parameters for Materials Under Non-isothermal Fatigue*, Honors in Major in Mechanical Engineering-Bachelors Thesis. University of Central Florida (2015).
21. T. Bouchenot, A.P. Gordon, S. Shinde, and P. Gravett, *Maer. Perform. Charact.* 3, 16 (2014).
22. T. Bouchenot, A.P. Gordon, S. Shinde, and P. Gravett, in *Proceedings of ASME Turbo Expo 2014: Turbine Technical Conference and Exposition*, ASME, Düsseldorf, Germany, (2014).
23. W. Ramberg and W.R. Osgood, Technical Note No. 902. National Advisory Committee for Aeronautics (1943).
24. G. Masing, in *Proceedings of the Second International Congress for Applied Mechanics*, Zurich, Switzerland, 332 (1926).
25. P.J., Armstrong and C.O. Frederick, *CEGB Report, RD/B/N731, Berkeley Nuclear Laboratories* (1966).
26. B. Clausen, D.W. Brown, J.S. Carpenter, K.D. Clarke, A.J. Clarke, S.C. Vogel, J.D. Bernardin, D. Spornjak, and J.M. Thompson, *Mater. Sci. Eng. A*. <https://doi.org/10.1016/j.msea.2017.04.081>.
27. H.J. Rack, Sandia National Laboratories Energy Report, 1 (1981).
28. H.M. Ledbetter, *J. Appl. Phys.* 52, 1587 (1981).

Publisher’s Note Springer Nature remains neutral with regard to jurisdictional claims in published maps and institutional affiliations.